

# Quality factors and dynamical tunneling in annular microcavities

Arnd Bäcker, Roland Ketzmerick, and Steffen Löck

*Institut für Theoretische Physik, Technische Universität Dresden, D-01062 Dresden, Germany*

Jan Wiersig

*Institut für Theoretische Physik, Universität Magdeburg, Postfach 4120, D-39016 Magdeburg, Germany*

Martina Hentschel

*Max-Planck-Institut für Physik komplexer Systeme,  
Nöthnitzer Straße 38, D-01187 Dresden, Germany*

(Dated: November 23, 2018)

The key characteristic of an optical mode in a microcavity is its quality factor describing the optical losses. The numerical computation of this quantity can be very demanding for present-day devices. Here we show for a certain class of whispering-gallery cavities that the quality factor is related to dynamical tunneling, a phenomenon studied in the field of quantum chaos. We extend a recently developed approach for determining dynamical tunneling rates to open cavities. This allows us to derive an analytical formula for the quality factor which is in very good agreement with full solutions of Maxwell's equations.

PACS numbers: 42.55.Sa, 42.60.Da, 05.45.Mt

## I. INTRODUCTION

Optical microcavities in which photons can be confined in three spatial dimensions are a subject of intensive research as they are relevant for applications, such as ultralow-threshold lasers [1, 2], single-photon emitters [3, 4] or correlated photon-pair emitters [5]. Especially whispering-gallery cavities such as microdisks [6, 7, 8], microspheres [9, 10], and microtoroids [11] have been investigated as they can trap photons for a long time near the boundary by total internal reflection. The corresponding whispering-gallery modes have a very high quality factor  $Q$ , which makes these cavities a candidate for the above-mentioned devices. While the microdisk emits the photons isotropically, cavities with deformed surfaces may additionally lead to directed emission [12, 13, 14, 15, 16, 17, 18, 19, 20, 21, 22, 23]. A particularly interesting geometry is the annular cavity [24, 25, 26] – a microdisk with a circular-shaped inclusion. A non-concentric (air) hole as inclusion allows for unidirectional emission and high quality factors simultaneously [17] which for most applications are desirable.

In this paper we connect the quality factors  $Q$  of optical microcavities to the concept of dynamical tunneling [27]. We provide an explicit prediction for the quality factors of whispering-gallery modes in the annular microcavity; see Fig. 1. Microcavities typically have a mixed phase space where regions of regular and chaotic motion coexist. Dynamical tunneling occurs between these dynamically separated phase-space regions. While for one-dimensional systems the tunneling process through an energetic barrier is well understood, e.g., by means of WKB theory [28], dynamical tunneling is a subject of intensive research experimentally [29, 30, 31] as well as theoretically [24, 32, 33, 34, 35, 36, 37, 38, 39, 40, 41, 42, 43, 44, 45]. Using a fictitious integrable system

[41], recently an approach has been developed [44, 45] which successfully predicts dynamical tunneling rates for quantum maps and billiards. In this paper we extend this approach to open optical microcavities, in particular to the annular cavity, to predict quality factors  $Q$  of whispering-gallery modes.

This paper is organized as follows. In Sec. II we introduce the annular cavity. In Sec. III we define the quality factors and derive the dynamical-tunneling contribution, which is then compared with numerical results. A summary is given in Sec. IV.

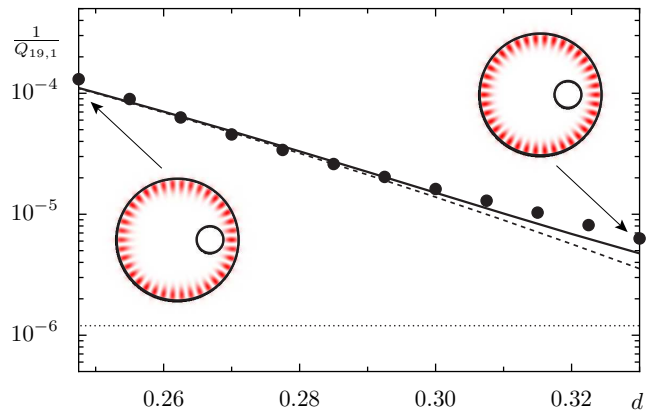


FIG. 1: (Color online) Inverse quality factors  $1/Q$  for the annular microcavity with refractive index  $n_{\text{eff}} = 2.0$ . Shown is the theoretical prediction (solid line), which is the sum of the direct tunneling contribution (dotted line) and the dynamical tunneling contribution (dashed line, Eq. (15)), and numerical data (dots) for angular quantum number  $m = 19$  and radial quantum number  $n = 1$  vs the hole position  $d$ . The insets show the resonant state at  $d = 0.2475$  and  $d = 0.33$ .

## II. ANNULAR MICROCAVITIES

Optical cavities are described by Maxwell's equations which in the case of quasi-two-dimensional microdisks reduce to a two-dimensional scalar mode equation [46]

$$-\nabla^2\psi = n^2(x,y)k^2\psi \quad (1)$$

with (effective) index of refraction  $n(x,y)$ , wave number  $k = \omega/c$ , frequency  $\omega$ , and the speed of light in vacuum  $c$ . The mode equation (1) is valid for both transverse magnetic (TM) and transverse electric (TE) polarization. We focus on TM polarization with the electric field  $\vec{E}(x,y,t) = (0,0,\psi(x,y)e^{-i\omega t})$  perpendicular to the cavity plane. The wave function  $\psi$  and its normal derivative are continuous across the boundary of the cavity. At infinity, only outgoing-wave components are allowed.

The mode equation (1) with the above-mentioned boundary conditions has analytical solutions only for special geometries such as the circle (see the Appendix) or several concentric circles. General geometries require numerical schemes such as the boundary element method [47] which we use in this paper. In this approach the two-dimensional partial differential equation (1) is rewritten as a one-dimensional integral equation involving Green's functions. Outgoing-wave conditions can be easily fulfilled by using the outgoing solution for the Green's functions. The boundary element method turns out to be very efficient even for computing highly excited modes and their quality factors.

A particularly suited example to study the influence of a mixed phase space onto the quality factors  $Q$  is the annular cavity. Its geometry is given by the radius  $R$  of the large disk, the radius  $R_2$  of the small disk and the minimal distance between the two disks  $d$ , see Fig. 2(a). Without loss of generality we choose  $R = 1$ . Under the variation in the two parameters  $d$  and  $R_2$  the dynamics inside the cavity changes drastically from completely regular behavior when the two disks are concentric ( $d = R - R_2$ ) to mixed regular-chaotic behavior for the general eccentric case. This is clearly visible for different trajectories in the Poincaré section, see Fig. 2(b). The Poincaré section is a two-dimensional phase-space representation. Whenever the trajectory hits the cavity's boundary, its position  $s$  (arclength coordinate along the circumference) and tangential momentum  $p = \sin \chi$  (the angle of reflection  $\chi$  is measured from the surface normal) is recorded. The large disk has an effective refractive index  $n_{\text{eff}}$  while inside the small disk and outside of the cavity the refractive index is unity. For the visualization of the ray dynamics we used an annular cavity with hard wall boundary conditions at the outer disk, neglecting ray-splitting effects.

The annular cavity has been studied extensively in the context of quantum chaos [25], optomechanics [26], avoided resonance crossings and resonant tunneling [24]. For applications it is of high interest as it allows for unidirectional light emission from high- $Q$  modes which has been predicted by the authors in Ref. [17] and has been

confirmed in recent experiments [21]. The closed system with perfectly reflecting walls, i.e., the annular billiard, is a paradigm for dynamical tunneling [35, 38].

## III. QUALITY FACTORS

The quality factor  $Q$  of a mode in an open cavity is related to the corresponding resonance with complex wave number  $k = \text{Re}(k) + i\text{Im}(k)$  via

$$Q = -\frac{\text{Re}(k)}{2\text{Im}(k)}. \quad (2)$$

In the annular cavity the quality factor  $Q$  of a regular mode has two contributions which are assumed to be additive

$$\frac{1}{Q} = \frac{1}{Q_{\text{dir}}} + \frac{1}{Q_{\text{dyn}}}. \quad (3)$$

Here,  $Q_{\text{dir}}$  accounts for the direct coupling of the regular mode to the continuum, as in the case of the circular cavity, see the Appendix. Note that for this contribution the mixed phase-space structure induced by the small disk is irrelevant. The second contribution,  $Q_{\text{dyn}}$ , is given by dynamical tunneling from the regular mode to the chaotic sea, which for  $|p| < p_c$  is strongly coupled to the

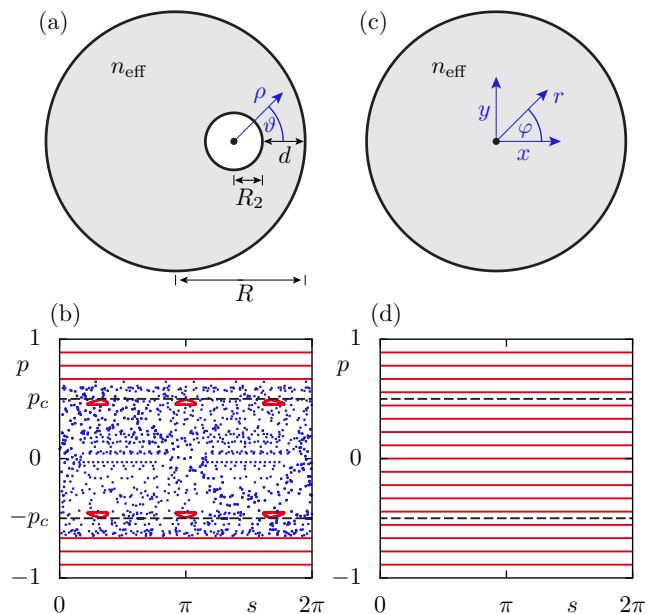


FIG. 2: (Color online) (a) Annular cavity with  $R = 1$ ,  $R_2 = 0.22$ , and  $d = 0.33$ . (b) Corresponding Poincaré section ( $s, p = \sin \chi$ ) for  $n_{\text{eff}} = 2.0$ , where  $s$  is the arclength along the boundary and  $\chi$  is the angle of reflection. Between the critical lines (dashed) with  $|p_c| = 1/n_{\text{eff}}$  is the leaky region, where the condition for total internal reflection is not fulfilled. (c) Circular cavity and (d) its completely regular phase space.

continuum, see Fig. 2(b). Here we assume that there are no further phase-space structures within the chaotic sea that affect the quality factor. A priori it is not obvious, which of these contributions will dominate.

### A. Dynamical tunneling contribution

We now want to derive a prediction for the dynamical tunneling contribution  $Q_{\text{dyn}}$  of regular modes in optical microcavities. After presenting the general approach we will apply it to the annular microcavity.

#### 1. General approach

We first review a quantum mechanical approach for determining dynamical tunneling rates using a fictitious integrable system [44, 45]; the relation to the quality factor  $Q_{\text{dyn}}$  will be given below. The tunneling rate  $\gamma$  of a regular state to the chaotic sea is described by Fermi's golden rule (using units  $\hbar = 2M = 1$ )

$$\gamma = 2\pi \langle |v| \rangle^2 \rho_{\text{ch}} \quad (4)$$

where  $\rho_{\text{ch}}$  denotes the density of chaotic states and  $\langle |v| \rangle^2$  is the averaged squared matrix element between the considered regular state and the chaotic states of similar energy. According to the Weyl formula for closed two-dimensional billiards the density of chaotic states is given by  $\rho_{\text{ch}} \approx A_{\text{ch}}/(4\pi)$ , where  $A_{\text{ch}}$  is the area of the billiard times the fraction of the chaotic phase-space volume. The eigenmodes of a system with a mixed phase space are mainly regular or chaotic, i.e., concentrated on a torus inside the regular region or spread out over the chaotic component. To calculate the coupling matrix elements  $v$  these so-called regular and chaotic eigenmodes cannot be used as they have small, but still too large, admixtures of the other type of modes compared to the tunneling rate. Instead, we determine  $v$  by introducing a fictitious integrable system  $H_{\text{reg}}$  as it was first suggested for dynamical tunneling in Ref. [41].  $H_{\text{reg}}$  has to be chosen such that its classical dynamics resembles the regular dynamics of the mixed system as closely as possible and extends it to phase space regions where  $H$  has a chaotic sea. The eigenstates  $\psi_{\text{reg}}$  of  $H_{\text{reg}}$  are localized in the regular region of  $H$  and decay into the chaotic sea of  $H$ . With chaotic states  $\psi_{\text{ch}}$ , which live in the chaotic region of phase space, the coupling matrix element is given as [44, 45, 48]

$$v = \int_{\mathbb{R}^2} \psi_{\text{ch}}^*(x, y) (H - H_{\text{reg}}) \psi_{\text{reg}}(x, y) dx dy. \quad (5)$$

Note that this equation is applicable for general systems but the determination of a sufficiently accurate  $H_{\text{reg}}$  is a difficult task. As previously mentioned we assume that there are no further phase-space structures within the chaotic sea that affect the tunneling rates  $\gamma$ . This approach was previously used to predict tunneling rates for quantum maps [44] and closed billiard systems [45].

The described approach can be extended to open cavities in the following way: (i) as a fictitious integrable system  $H_{\text{reg}}$  we choose a cavity such that it resembles the regular dynamics of  $H$ . The quantum system has resonance states  $\psi_{\text{reg}}$ . (ii) As a model for the chaotic resonances  $\psi_{\text{ch}}$  a random wave model will be used, which in addition fulfills the relevant cavity boundary conditions. (iii) The tunneling rate  $\gamma$  determines the quality factor  $Q_{\text{dyn}}$  by

$$Q_{\text{dyn}} = \frac{2\text{Re}(k)^2 n_{\text{eff}}^2}{\gamma} \quad (6)$$

where we used the quantum mechanical relation between energy and momentum  $E_0 - i\frac{\gamma}{2} = p^2$ , with  $p = n_{\text{eff}}k$  in a refractive medium such that  $\gamma = -2n_{\text{eff}}^2 \text{Im}(k^2) = -4n_{\text{eff}}^2 \text{Re}(k) \text{Im}(k)$ .

#### 2. Application to the annular cavity

To evaluate Eq. (5) we have to find an appropriate regular system  $H_{\text{reg}}$ . For the annular cavity a natural choice is given by the circular cavity as it correctly reproduces the regular whispering-gallery motion of the annular cavity and extends it into the chaotic region of phase space. The whispering-gallery modes are labeled by the two quantum numbers  $m$  and  $n$ . Rewriting the mode equation (1) as an eigenvalue equation  $H\psi = k^2\psi$  the Hamiltonian of the annular cavity can be introduced as

$$H = -\nabla^2 + [1 - n(x, y)^2]k^2 \quad (7)$$

where the refractive index  $n(x, y)$  is  $n_{\text{eff}}$  inside and 1 outside the cavity and in the disk of radius  $R_2$ . As the regular system  $H_{\text{reg}}$  we choose the circular cavity

$$H_{\text{reg}} = -\nabla^2 + [1 - n_{\text{reg}}(x, y)^2]k^2 \quad (8)$$

where the refractive index  $n_{\text{reg}}(x, y)$  is  $n_{\text{eff}}$  inside and 1 outside the circular cavity. Thus  $H$  and  $H_{\text{reg}}$  differ only inside the small disk of radius  $R_2$  with  $H - H_{\text{reg}} = (1 - n_{\text{eff}}^2)k^2$  and the integral in Eq. (5) reduces to an integral over the small disk. For the regular states inside the circular cavity we choose, as in the numerical studies, the even eigenmodes

$$\psi_{\text{reg}}^{mn}(r, \varphi) = N_{mn} J_m(n_{\text{eff}} k_{mn} r) \cos(m\varphi) \quad (9)$$

where  $k_{mn}$  are the complex resonant wave numbers, according to the Appendix, and  $\psi_{\text{reg}}^{mn}$  is normalized to one with the numerically determined normalization constant  $N_{mn}$ .

To model the chaotic modes  $\psi_{\text{ch}}$  within the small disk we employ a random wave description [49], which has been extended to systems with a mixed phase space [50]. While this model accurately describes the random behavior in a medium with constant refractive index, it cannot account for the change in refractive index at the border of

the small disk at  $\rho = R_2$ . We extend a boundary-adapted random wave model [51] to account for this boundary condition. This is essential especially for low  $\text{Re}(k)$  as then all chaotic modes decay inside the small disk, which cannot be reproduced by the usual random wave model. Therefore we construct the chaotic states  $\psi_{\text{ch}}$  as a random superposition of modes of a circular cavity of radius  $R_2$  with refractive index 1 which is surrounded by a medium with refractive index  $n_{\text{eff}}$ . As follows from Eq. (19) these modes, at a fixed complex wave number  $k_{mn}$  and within the small disk, are

$$\psi_l(\rho, \vartheta) = A_l J_l(k_{mn}\rho) \cos(l\vartheta), \quad \rho \leq R_2. \quad (10)$$

The chaotic states  $\psi_{\text{ch}}$  are then constructed by a random superposition of these modes

$$\psi_{\text{ch}}(\rho, \vartheta) = \frac{1}{\sqrt{A_{\text{ch}}}} \sum_{l=1}^{\infty} a_l \psi_l(\rho, \vartheta). \quad (11)$$

Here the coefficients  $a_l$  are Gaussian random variables with mean zero and  $\langle a_l a_k \rangle = \delta_{l,k}$ . The random waves, constructed in such a way, fulfill the normalization condition  $\langle |\psi_{\text{ch}}|^2 \rangle = 1/A_{\text{ch}}$  required for the annular cavity.

Using the fictitious regular system and the random wave model for the chaotic states we obtain an integral over the small disk for the coupling matrix element

$$v_{mn} = \int_0^{R_2} \int_0^\pi \rho \, d\rho \, d\vartheta \, \psi_{\text{ch}}^*(\rho, \vartheta) (1 - n_{\text{eff}}^2) k_{mn}^2 \psi_{\text{reg}}(\rho, \vartheta). \quad (12)$$

For the tunneling rate this results in

$$\gamma_{mn} = \frac{1}{2} N_{mn}^2 (1 - n_{\text{eff}}^2)^2 |k_{mn}^2|^2 \sum_{l=1}^{\infty} |I_l|^2 \quad (13)$$

where

$$I_l = \int_0^{R_2} \int_0^\pi \rho \, d\rho \, d\vartheta \, \psi_l^*(\rho, \vartheta) J_m(n_{\text{eff}} k_{mn} r) \cos(m\varphi) \quad (14)$$

with  $r = r(\rho, \vartheta)$  geometrically related to  $\varphi = \varphi(\rho, \vartheta)$ , see Figs. 2(a) and (c). With Eq. (6) we finally obtain the dynamical tunneling contribution to the quality factor

$$Q_{\text{dyn}}^{mn} = \frac{4n_{\text{eff}}^2}{N_{mn}^2 (1 - n_{\text{eff}}^2)^2 |k_{mn}^2| \sum_{l=1}^{\infty} |I_l|^2} \quad (15)$$

of whispering-gallery modes in the annular microcavity for each quantum number  $m$  and  $n$ .

## B. Results

Now we compare our theoretical prediction for the quality factor, Eq. (3), for the annular microcavity with numerical data, obtained using the boundary element method [47]. Figure 1 shows the inverse quality factors

at fixed quantum numbers  $m = 19$  and  $n = 1$  under variation in the distance  $d$  between the small and the large disk. The direct contribution  $1/Q_{\text{dir}}$ , see the Appendix, is independent of the distance  $d$ . It is dominated by the dynamical tunneling contribution  $1/Q_{\text{dyn}}$ , Eq. (15), which decreases exponentially with  $d$ , as expected from the increasing regular phase space region. We find excellent agreement of the prediction and the numerical data.

As a further test we consider the quality factors for fixed radial quantum number  $n = 1$  and increasing angular quantum number  $m = 7, \dots, 21$ , comparing the theoretical prediction with numerical results, see Fig. 3. We find that for small  $\text{Re}(k)$  the direct tunneling from the whispering-gallery modes to the continuum is relevant while for large  $\text{Re}(k)$  the dynamical-tunneling contribution dominates. Here, our prediction again shows excellent agreement with the numerical data. Note that for other systems, such as the one considered in Ref. [42], only  $Q_{\text{dyn}}$  may be the relevant contribution. Also we point out, that our theory allows to determine quality factors for large  $\text{Re}(k)$ , where numerical methods fail. The boundary element method cannot compute the quality factors of quantum numbers  $n = 1$  and  $m > 21$  reliably as the exponentially increasing quality factor requires an extremely fine spatial discretization.

## C. Additional phase space structures

In the derivation of the dynamical tunneling contribution  $1/Q_{\text{dyn}}$  to the quality factor we assumed that there are no further structures in the chaotic part of phase space, such as small regular islands and partial barriers.

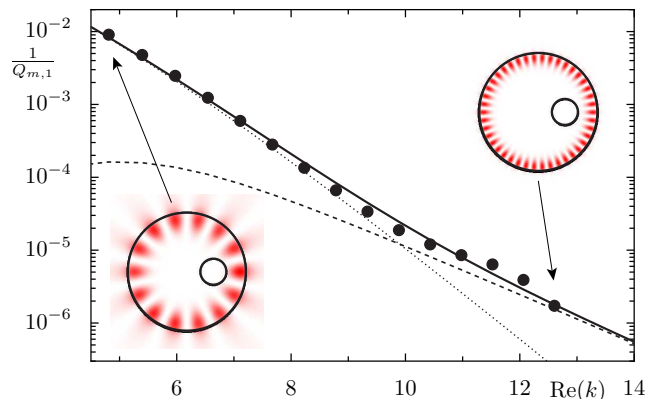


FIG. 3: (Color online) Inverse quality factors  $1/Q$  for the annular microcavity with  $n_{\text{eff}} = 2.0$ . Shown is the theoretical prediction (solid line) which is the sum of the direct tunneling contribution (dotted line) and the dynamical tunneling contribution (dashed line, Eq. (15)), and numerical data (dots) for  $m = 7, \dots, 21$  and  $n = 1$  at  $d = 0.33$ . The insets exemplarily show the resonant states of angular quantum number  $m = 7$  (left) and  $m = 21$  (right).

If this assumption is not fulfilled, the tunneling rate  $\gamma$  is modified and consequently the quality factor.

This can be demonstrated when choosing  $d = 0.33$ ,  $R_2 = 0.22$ , and increasing  $n_{\text{eff}}$  from 2.0 to 2.3. At  $n_{\text{eff}} = 2.0$  no visible additional structures exist in the chaotic part of phase space above the critical line (see Fig. 2(b)). At  $n_{\text{eff}} = 2.3$  the critical line  $p_c$  is shifted to smaller values and a period-three island chain is now above  $p_c$  as can be seen in the inset in Fig. 4. These structures presumably cause the oscillations on top of the numerically determined quality factors that are visible in Fig. 4. To support the conjecture, that the island chain is responsible for the oscillations, Figs. 5(a) and 5(b) display the incident Husimi functions [52], representing the wave analog of the Poincaré section (see also [53]), of the mode  $m = 14$  (near the minimum of the oscillation) and  $m = 18$  (near the maximum). In the former case the island chain is clearly a barrier for the mode. The mode cannot penetrate the leaky region so easily, which increases its quality factor. In the latter case the island chain seems not to have a strong influence on the mode. While the average behavior of the quality factors is still well predicted by Eq. (15), these oscillations cannot be explained by our theory as it assumes a strong coupling of the chaotic modes to the continuum. Other situations where this coupling is weak are due to dynamical localization [54] or to an additional tunnel barrier surrounding a cavity [24]. We leave the interesting task of the prediction of tunneling rates through more complicated phase-space structures in the chaotic sea as a future challenge.

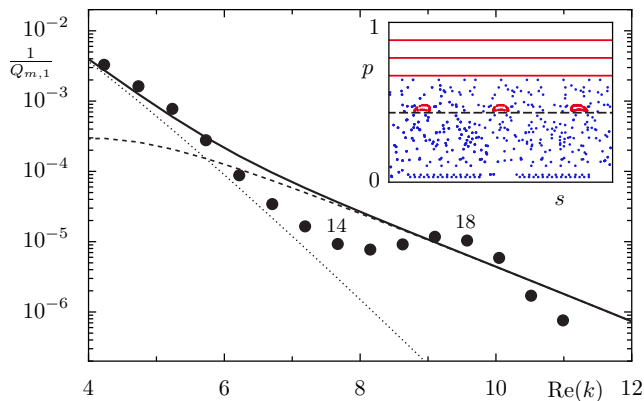


FIG. 4: (Color online) Inverse quality factor  $1/Q$  for the annular microcavity. Shown is the theoretical prediction (solid line) which is the sum of the direct tunneling contribution (dotted line) and the dynamical tunneling contribution (dashed line), and numerical data (dots) for  $m = 7, \dots, 21$ ,  $n = 1$  at  $d = 0.33$  and  $n_{\text{eff}} = 2.3$ . The inset shows a Poincaré section of the classical phase space, where the critical line  $p = p_c$  is marked (dashed line).

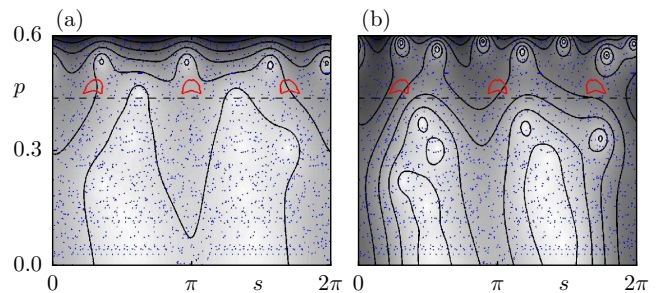


FIG. 5: (Color online) Husimi functions (gray scale and contour lines) of the modes with angular quantum number (a)  $m = 14$  and (b)  $m = 18$  superimposed onto part of the Poincaré section of the classical phase space, where the critical line  $p = p_c$  is marked (dashed line). The radial quantum number is  $n = 1$  and the refractive index is  $n_{\text{eff}} = 2.3$  as in Fig. 4.

#### IV. SUMMARY

We have presented a theory for the intrinsic optical losses of annular microcavities. It is assumed that the ray dynamical phase space is divided into regular regions and a chaotic region which does not show additional structures such as small regular islands or partial barriers. Our theory gives an analytical expression for the quality factor which is in very good agreement with the full numerical simulations of Maxwell's equations. We would like to emphasize that our theory can predict quality factors also in the regime of large wave numbers where numerical methods fail due to the exponential increase in the quality factor.

#### Acknowledgments

Financial support from the DFG research group 760 and the DFG Emmy Noether Programme is acknowledged.

#### APPENDIX: THE CIRCULAR MICROCAVITY

For completeness, let us consider a circular microcavity of radius  $a$  in more detail. Inside the cavity the refractive index is denoted by  $n_1$  and outside by  $n_2 < n_1$  (see Fig. 2(c)). In the classical ray picture trajectories stay inside the cavity if their angle of incidence with the boundary is larger than the angle of total internal reflection  $\arcsin(n_2/n_1)$ . The dynamics is completely regular. The circular cavity in TM-polarization is described by the Schrödinger equation in polar coordinates  $(r, \varphi)$

$$-\nabla^2 \psi(r, \varphi) = n(r)^2 k^2 \psi(r, \varphi) \quad (16)$$

where  $n(r)$  changes from  $n_1$  inside to  $n_2$  outside the cavity. The radial and the angular part can be separated,

using the ansatz  $\psi(r, \varphi) = u(r)\phi(\varphi)$ . We immediately obtain  $\phi(\varphi) = e^{im\varphi}$ , where  $m \in \mathbb{Z}$  denotes the angular quantum number. The radial part

$$-\left(\frac{\partial^2}{\partial r^2} + \frac{1}{r} \frac{\partial}{\partial r}\right)u(r) + V_{\text{eff}}(r)u(r) = k^2u(r) \quad (17)$$

describes the motion of a particle in an effective potential

$$V_{\text{eff}}(r) = k^2[1 - n(r)^2] + \frac{m^2}{r^2}. \quad (18)$$

Metastable states inside this potential exist for  $m/(n_1a) < k < m/(n_2a)$  and correspond to states with evanescent leakage that, in the ray picture, are fully confined by total internal reflection. The solutions of the radial equation are given as

$$u(r) = \begin{cases} A_m J_m(n_1kr), & r < a \\ H_m^{(2)}(n_2kr) + S_m H_m^{(1)}(n_2kr), & r > a \end{cases} \quad (19)$$

where the incoming wave is described by the Hankel function of the second kind  $H_m^{(2)}(n_2kr)$  and the scattered one is described by the Hankel function of the first kind  $S_m H_m^{(1)}(n_2kr)$  with a certain scattering amplitude  $S_m$ .  $A_m$  describes the amount of probability entering the cavity. Using that the radial solutions and their derivative have to be continuous at  $r = a$  and that the scattering matrix has a pole at a resonance position, this complex resonance position  $k = \text{Re}(k) + i\text{Im}(k)$  can be found by numerically solving

$$n_1 J_{m+1}(n_1ka) H_m^{(1)}(n_2ka) = n_2 J_m(n_1ka) H_{m+1}^{(1)}(n_2ka) \quad (20)$$

for complex  $k$ . From this  $Q_{\text{dir}} = -\text{Re}(k)/[2\text{Im}(k)]$  is obtained.

- 
- [1] H.-G. Park, S.-H. Kim, S.-H. Kwon, Y.-G. Ju, J.-K. Yang, J.-H. Baek, S.-B. Kim, and Y.-H. Lee, *Science* **305**, 1444 (2004).
- [2] S. M. Ulrich, C. Gies, S. Ates, J. Wiersig, S. Reitzenstein, C. Hofmann, A. Löffler, A. Forchel, F. Jahnke, and P. Michler, *Phys. Rev. Lett.* **98**, 043906 (2007).
- [3] J. Kim, O. Benson, H. Kan, and Y. Yamamoto, *Nature* **397**, 500 (1999).
- [4] P. Michler, A. Imamoglu, M. D. Mason, P. J. Carson, G. F. Strouse, and S. K. Buratto, *Nature* **406**, 968 (2000).
- [5] M. Benyoucef, S. M. Ulrich, P. Michler, J. Wiersig, F. Jahnke, and A. Forchel, *J. Appl. Phys.* **97**, 023101 (2005).
- [6] S. L. McCall, A. F. J. Levi, R. E. Slusher, S. J. Pearton, and R. A. Logan, *Appl. Phys. Lett.* **60**, 289 (1992).
- [7] C. P. Michael, K. Srinivasan, T. J. Johnson, O. Painter, K. H. Lee, K. Hennessy, H. Kim, and E. Hu, *Appl. Phys. Lett.* **90**, 051108 (2007).
- [8] T. J. Kippenberg, J. Kalkman, A. Polman, and K. J. Vahala, *Phys. Rev. A* **74**, 051802(R) (2006).
- [9] L. Collot, V. Lefèvre-Seguin, M. Brune, J. M. Raimond, and S. Haroche, *Europhys. Lett.* **23**, 327 (1993).
- [10] S. Götzinger, L. d. S. Menezes, A. Mazzei, S. Kühn, V. Sandoghar, and O. Benson, *Nano Lett.* **6**, 1151 (2006).
- [11] D. K. Armani, T. J. Kippenberg, S. M. Spillane, and K. J. Vahala, *Nature* **421**, 925 (2003).
- [12] A. F. J. Levi, R. E. Slusher, S. L. McCall, J. L. Glass, S. J. Pearton, and R. A. Logan, *Appl. Phys. Lett.* **62**, 561 (1993).
- [13] J. U. Nöckel and A. D. Stone, *Nature (London)* **385**, 45 (1997).
- [14] C. Gmachl, F. Capasso, E. E. Narimanov, J. U. Nöckel, A. D. Stone, J. Faist, D. L. Sivco, and A. Y. Cho, *Science* **280**, 1556 (1998).
- [15] M. S. Kurdoglyan, S.-Y. Lee, S. Rim, and C.-M. Kim, *Opt. Lett.* **29**, 2758 (2004).
- [16] M. Kneissl, M. Teepe, N. Miyashita, N. M. Johnson, G. D. Chern, and R. K. Chang, *Appl. Phys. Lett.* **84**, 2485 (2004).
- [17] J. Wiersig and M. Hentschel, *Phys. Rev. A* **73**, 031802(R) (2006).
- [18] T. Tanaka, M. Hentschel, T. Fukushima, and T. Harayama, *Phys. Rev. Lett.* **98**, 033902 (2007).
- [19] J. Wiersig and M. Hentschel, *Phys. Rev. Lett.* **100**, 033901 (2008).
- [20] Q. Song, H. Cao, B. Liu, S. T. Ho, W. Fang, and G. S. Solomon, arXiv0810.3923 (2008).
- [21] F. Wilde, Ph.D. thesis, University of Hamburg, Germany (2008).
- [22] C. Yan, Q. Wang, L. Diehl, M. Hentschel, J. Wiersig, N. Yu, C. Pflüg, M. A. Belkin, M. Yamanishi, H. Kan, et al., to be submitted (2009).
- [23] M. Hentschel and T.-Y. Kwon, *Opt. Lett.* **34**, 163 (2009).
- [24] G. Hackenbroich and J. U. Nöckel, *Europhys. Lett.* **39**, 371 (1997).
- [25] M. Hentschel and K. Richter, *Phys. Rev. E* **66**, 056207 (2002).
- [26] H. Schomerus, J. Wiersig, and M. Hentschel, *Phys. Rev. A* **70**, 012703 (2004).
- [27] M. J. Davis and E. J. Heller, *J. Chem. Phys.* **75**, 246 (1981).
- [28] E. Merzbacher, *Quantum Mechanics* (Wiley, New York, 1998).
- [29] D. A. Steck, W. H. Oskay, and M. G. Raizen, *Science* **293**, 274 (2001).
- [30] W. K. Hensinger, H. Häffner, A. Browaeys, N. R. Heckenberg, K. Helmerson, C. McKenzie, G. J. Milburn, W. D. Phillips, S. L. Rolston, H. Rubinsztein-Dunlop, et al., *Nature* **412**, 52 (2001).
- [31] T. M. Fromhold, P. B. Wilkinson, R. K. Hayden, L. Eaves, F. W. Sheard, N. Miura, and M. Henini, *Phys. Rev. B* **65**, 155312 (2002).
- [32] J. D. Hanson, E. Ott, and T. M. Antonsen, *Phys. Rev. A* **29**, 819 (1984).
- [33] M. Wilkinson, *Physica (Amsterdam) D* **21**, 341 (1986).
- [34] O. Bohigas, S. Tomsovic, and D. Ullmo, *Phys. Rep.* **223**, 43 (1993).
- [35] O. Bohigas, D. Boosé, R. Eglydio de Carvalho, and

- V. Marvulle, Nucl. Phys. A **560**, 197 (1993).
- [36] S. Tomsovic and D. Ullmo, Phys. Rev. E **50**, 145 (1994).
- [37] A. Shudo and K. S. Ikeda, Phys. Rev. Lett. **74**, 682 (1995).
- [38] E. Doron and S. D. Frischat, Phys. Rev. Lett. **75**, 3661 (1995); S. D. Frischat and E. Doron, Phys. Rev. E **57**, 1421 (1998).
- [39] S. Tomsovic, J. Phys. A **31**, 9469 (1998).
- [40] S. C. Creagh, *Tunneling in Complex Systems*, in *Tunneling in Complex Systems* (World Scientific, Singapore, 1998).
- [41] V. A. Podolskiy and E. E. Narimanov, Phys. Rev. Lett. **91**, 263601 (2003).
- [42] V. A. Podolskiy and E. E. Narimanov, Opt. Lett. **30**, 474 (2005).
- [43] M. Sheinman, S. Fishman, I. Guarneri, and L. Rebuzzini, Phys. Rev. A **73**, 052110 (2006).
- [44] A. Bäcker, R. Ketzmerick, S. Löck, and L. Schilling, Phys. Rev. Lett. **100**, 104101 (2008).
- [45] A. Bäcker, R. Ketzmerick, S. Löck, M. Robnik, G. Vidmar, R. Höhmann, U. Kuhl, and H.-J. Stöckmann, Phys. Rev. Lett. **100**, 174103 (2008).
- [46] J. D. Jackson, *Classical Electrodynamics* (Wiley and Sons, New York, 1962).
- [47] J. Wiersig, J. Opt. A: Pure Appl. Opt. **5**, 53 (2003).
- [48] A. Bäcker, R. Ketzmerick, and S. Löck, (unpublished).
- [49] M. V. Berry, J. Phys. A **10**, 2083 (1977).
- [50] A. Bäcker and R. Schubert, J. Phys. A **35**, 527 (2002).
- [51] M. V. Berry, J. Phys. A **35**, 3025 (2002).
- [52] M. Hentschel, H. Schomerus, and R. Schubert, Europhys. Lett. **62**, 636 (2003).
- [53] A. Bäcker, S. Furstberger, and R. Schubert, Phys. Rev. E **70**, 036204 (2004).
- [54] G. Casati, I. Guarneri, and D. L. Shepelyansky, Phys. Rev. A **36**, 3501 (1987).